

Breaking the Illusion: Consensus-Based Generative Mitigation of Adversarial Illusions in Multi-Modal Embeddings

Fatemeh Akbarian^{*‡}, Anahita Baninajjar^{*‡}, Yingyi Zhang^{*‡}, Ananth Balashankar[†], Amir Aminifar^{*}

^{*}Lund University, Sweden [†]Google DeepMind, USA

{fatemeh.akbarian, anahita.baninajjar, yingyi.zhang, amir.aminifar}@eit.lth.se, ananthbshankar@google.com

Abstract—Multi-modal foundation models align images, text, and other modalities in a shared embedding space but remain vulnerable to adversarial illusions [35], where imperceptible perturbations disrupt cross-modal alignment and mislead downstream tasks. To counteract the effects of adversarial illusions, we propose a task-agnostic mitigation mechanism that reconstructs the input from the attacker’s perturbed input through generative models, e.g., Variational Autoencoders (VAEs), to maintain natural alignment. To further enhance our proposed defense mechanism, we adopt a generative sampling strategy combined with a consensus-based aggregation scheme over the outcomes of the generated samples. Our experiments on the state-of-the-art multi-modal encoders show that our approach substantially reduces the illusion attack success rates to near-zero and improves cross-modal alignment by 4% (42 → 46) and 11% (32 → 43) in unperturbed and perturbed input settings respectively, providing an effective and model-agnostic defense against adversarial illusions.

Index Terms—Multi-modal embeddings, Adversarial illusions, Generative sampling, Aggregation

I. INTRODUCTION

Multi-modal foundation models have rapidly advanced the frontier of visual and linguistic understanding. Foundation models such as CLIP [19], ALIGN [11], and ImageBind [8] align a variety of heterogeneous modalities including images, text, and other modalities within a shared embedding space, thereby enabling zero-shot classification, cross-modal retrieval, and generative conditioning.

The shared embedding space that underpins cross-modal flexibility simultaneously introduces a new attack surface, giving rise to *adversarial illusions* [35]. As downstream tasks directly rely on the integrity of this shared representation, even small perturbations in one modality can induce semantic misalignment across others, misleading models that depend on the embedding for retrieval, captioning, or generative conditioning. Defending against such cross-modal attacks presents unique challenges. Conventional adversarial defenses, originally developed for unimodal classifiers, emphasize local decision-boundary robustness [2, 9, 16, 26]. However, these techniques fail to maintain alignment in the shared embedding space. Even if accuracy is preserved, the perturbed features may still project to semantically inconsistent regions in the

shared embedding space [29, 35, 36]. This misalignment undermines downstream tasks such as captioning, retrieval, and conditional generation, where maintaining cross-modal coherence is essential.

Existing defenses against adversarial perturbations remain limited in multi-modal settings. Preprocessing methods such as feature squeezing and JPEG compression [10, 32] can suppress pixel-level noise but do not restore cross-modal alignment. Adversarial and diffusion-based training schemes improve robustness within individual modalities [7, 22], yet require retraining and often reduce clean performance. To the best of our knowledge, no post-hoc, task-agnostic defense mechanism has been shown to restore cross-modal embedding alignment after adversarial illusions, underscoring the need for new mitigation mechanisms targeting multi-modal embeddings.

In this paper, we propose a post-hoc task-agnostic mitigation mechanism against adversarial illusions. Our proposed mitigation processes adversarially perturbed inputs through a generative model such as autoencoders (AEs), variational autoencoders (VAEs), or diffusion models (DMs) to reconstruct the input from the attacker’s perturbed input. By reconstructing the inputs on a learned data manifold, these models suppress adversarial perturbations and project them back onto the natural cross-modal alignment. This generative reconstruction framework mitigates adversarial illusions, restoring semantic consistency across modalities and preserving coherence in cross-modal generation.

To further enhance our proposed mitigation mechanism, we adopt a generative sampling strategy combined with a consensus-based aggregation scheme over the outcomes of the generated samples. Generative sampling is the process of drawing multiple input reconstructions from a generative model, e.g., a VAE, conditioned on a given input. This generative sampling and aggregation scheme, further enhances robustness by leveraging the diversity of stochastic reconstructions to mitigate adversarial illusions and restore cross-modal alignment. The result is a post-hoc task-agnostic defense that is both model-independent and scalable across modalities.

We perform extensive experiments to demonstrate the effectiveness of our mitigation mechanism. First, our proposed mitigation improves the classification accuracy of the downstream task even when there is no adversarial illusions, from 42%/66% to 46%/73% in Top-1/Top-5 accuracies, respec-

[‡] Equal contribution.

[†] Contributed in an advisory role.

tively. Second, our proposed mitigation effectively neutralizes the attacker’s attempt to alter the downstream task’s prediction toward the targeted label, reducing the attack success rate from 62%/90% in Top-1/Top-5 accuracies to only 0%/2%, respectively. Finally, our proposed mitigation not only effectively counteracts the attacker’s effort to steer the downstream task’s prediction toward the targeted label, but also realigns the perturbed input with the correct/original label, outperforming the state of the art, with Top-1/Top-5 accuracies improved from 32%/56% (for the best mitigation in [35]) to 43%/68%, respectively. We summarize our main contributions as follows:

- We propose an effective mitigation mechanism against adversarial illusions in multi-modal embeddings based on a generative sampling strategy (using AEs, VAEs, or DMs) combined with a consensus-based aggregation scheme over the generated samples (using majority voting).
- We extensively evaluate our proposed mitigation mechanism against the state of the art and demonstrate that our proposed mitigation effectively restore cross-modal alignment under adversarial illusion attacks. For perturbed images, the cosine similarity with the correct text labels improves from 0.11 ± 0.05 (no mitigation) to 0.82 ± 0.07 , while the Top-1/Top-5 accuracies increases from 0%/0% to 43%/68%, substantially reducing adversarial illusion success rates without requiring retraining.

II. MITIGATION FRAMEWORK

In this section, we begin by detailing the threat model and explaining how the attacker manipulates cross-modal representations to induce semantic misalignment in adversarial illusion attack. Then, we introduce the goal of mitigating adversarial illusion attacks, while retaining cross-modal alignment on unperturbed inputs. We then describe our *consensus-based generative mitigation*, which achieves this goal by projecting perturbed inputs back toward the natural data manifold before inference.

A. Threat Model

Adversarial illusion [35] is a targeted multi-modal attack where imperceptible perturbations are applied to an input to corrupt its genuine cross-modal alignment. By manipulating the shared embedding space, the attacker can steer any input to align closely with an arbitrary target sample from another modality, thereby inducing consistent semantic misalignment across downstream tasks.

The overview of the adversarial illusion attack is shown in Figure 1. The adversarial illusion attack is achieved through an iterative optimization process (red arrows in Figure 1) using Projected Gradient Descent (PGD), which updates the perturbation to maximize the Cosine Similarity (CS) between the embeddings of the perturbed input image and the designated target text (i.e., “a man in a prison cell” in this example). This formulation makes the adversarial illusion task-agnostic, as it operates directly in the shared embedding space rather than relying on any specific downstream task such as

classification, retrieval, or generation. The adversarial illusion explicitly targets the embedding space of multi-modal models, exploiting the interchangeability of representations across modalities to induce cross-domain misalignment. Moreover, it exhibits strong transferability where illusions generated using one encoder remain effective across models with different encoders.

B. Consensus-Based Generative Mitigation

Mitigation Goal: Given clean or unperturbed inputs, and perturbed inputs generated to induce adversarial illusions in multi-modal embeddings; our goal is to two-part: (1) *Minimize adversarial illusion attack success rates*; (2) *Retain cross-modal alignment on unperturbed inputs; in a model and task agnostic manner*.

This formulation ensures that a mitigation approach does not reduce the utility of the multi-modal models in benign settings - thus rendering them useless, in the process of improving robustness to adversarial illusion attacks. Further, achieving this goal in a model or task agnostic defense, ensures that a mitigation approach can scale seamlessly to many downstream applications.

To achieve this goal, we leverage how adversarial illusions operate by driving the input representation toward an incorrect target in the shared embedding space. Our defense focuses on restoring the original alignment without altering the encoder or retraining downstream models. To this end, we propose a consensus-based generative sampling framework that reconstructs sanitized inputs from adversarially perturbed samples prior to inference, aiming to recover representations consistent with the natural cross-modal structure. As illustrated in Figure 1, the framework combines generative reconstruction with stochastic sampling to guide perturbed inputs back toward the natural data manifold. This reconstruction step not only removes the adversarial shift toward the attacker’s target but also maintains the prediction that the clean input would have produced, ensuring that the intended semantic label is preserved.

To ensure that our approach is model and task agnostic, we build our defense on top of pretrained generative models, rather than training a new reconstructor, because these models already approximate the natural image manifold and are widely available in multi-modal pipelines. They allow us to sanitize inputs with minimal system changes as they naturally suppress off-manifold perturbations that adversarial illusions rely on. Using an off-the-shelf generator as a projection step lets us wrap the encoder with a lightweight defense, even when we only have black-box access to the downstream system.

We now detail how the generative model transforms an adversarial input into a sanitized reconstruction. Given an adversarial input $\tilde{x} = x + \delta$, where δ denotes a small imperceptible perturbation crafted to disrupt alignment, our objective is to recover a sanitized input \hat{x} whose representation preserves the semantics of the original input x . A generative model \mathcal{G}_θ , e.g., AE, VAE, or DM, acts as a post-hoc sanitizer

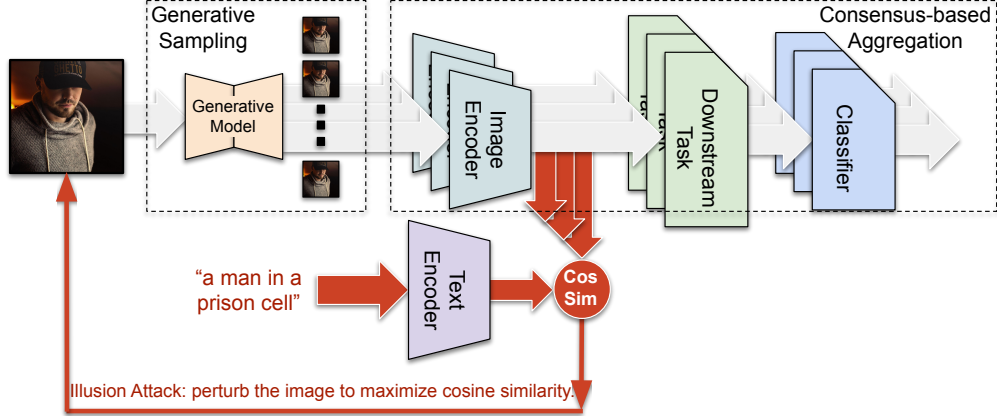


Fig. 1. Overview of our consensus-based generative sampling mitigation framework. Our mitigation scheme has two main components: a generative sampling and a consensus-based aggregation. The generative sampling mechanism adopts a generative model to reconstruct several variants of the input image. The consensus-based aggregation mechanism aggregates the decisions for the generated samples, e.g., based on majority voting. The red arrows describe the illusion attack, where the adversary attempts to maximize the cosine similarity between the embedding of the perturbed image and the embedding of the target text (i.e., “a man in a prison cell” in this example).

that reconstructs sanitized inputs from adversarially perturbed samples, where

$$\hat{x} = \mathcal{G}_\theta(\tilde{x}).$$

This reconstruction maps the adversarial input into a low-dimensional latent space and decodes it back to the natural input domain. Thus, \mathcal{G}_θ provides a smooth approximation of the underlying data manifold, suppressing high-frequency, off-manifold perturbations that induce misalignment in the shared embedding space.

Beyond deterministic reconstruction, we leverage the stochastic nature of generative models enables further robustness through sampling and aggregation. Given an adversarial input \tilde{x} , we draw N independent reconstructions such that

$$\hat{x}_i = \mathcal{G}_\theta(\tilde{x}, \epsilon_i), \quad \epsilon_i \sim \mathcal{N}(0, \sigma^2 I),$$

where ϵ_i denotes stochastic noise applied in the latent or diffusion space. Each reconstruction \hat{x}_i is evaluated by the downstream model to obtain a corresponding prediction $y_i = h(f(\hat{x}_i))$, where f is the multi-modal encoder and h the task-specific head, e.g., classifier or retrieval function. The final prediction is obtained via majority aggregation $\hat{y} = \text{mode}(\{y_i\}_{i=1}^N)$, where mode selects the label that appears most frequently among the reconstructed samples. This further reduces the probability of an illusion attack success to $\sum_{k=\lfloor \frac{N}{2} \rfloor + 1}^N \binom{N}{k} \eta^k (1 - \eta)^{N-k}$, where η is the diminished probability of an illusion attack persisting in one reconstructed sanitized input.

This consensus-based aggregation scheme leverages the diversity of generative reconstructions to reduce sensitivity to localized perturbations in input space. Our defense further benefits from the inductive bias of generative models, which constrain reconstructions to the natural data manifold. By integrating reconstruction, stochastic sampling, and majority aggregation, the method effectively smooths the decision

boundary in the shared embedding space, reducing the effective gradient available to the attacker. Consequently, small perturbations in input space no longer yield consistent alignment shifts across reconstructions, significantly enhancing robustness to adversarial illusions. Our proposed approach achieves the defense goal as it is post-hoc, task-agnostic, and model-independent, requiring no modification to the target encoder or downstream network.

III. IMPLEMENTATION SETUP

We evaluate our methods using the adversarial image–text pairs released with the Adversarial Illusions benchmark [35]. The dataset provides both *original* and *perturbed* images generated to induce targeted cross-modal misalignment in the **ImageBind** multi-modal embedding model. Each perturbed image is designed to align with an adversary-chosen target text while remaining visually similar to the original image.

Datasets: The benchmark is derived from ImageNet categories and includes paired original and perturbed images with their associated original and target labels. This structure enables controlled comparison of semantic alignment recovery across different mitigation methods.

Metrics: We report Cosine Similarity (CS) between image embeddings $f(x)$ and the correct label embeddings e_y (\uparrow is better), which captures how closely the two representations align, defined as follows,

$$\text{CS}(x, y) = \frac{f(x)^\top e_y}{\|f(x)\| \|e_y\|}.$$

We also evaluate Top-1 and Top-5 accuracy. Given model scores $s(x)$, the Top- k set is defined as: $\text{TopK}(x, k) = \text{argsort}(s(x))_{1:k}$. The correctness indicator is $\mathbf{1}_{\text{Top}k}(x, y) = \mathbb{I}[y \in \text{TopK}(x, k)]$. Top-1 reflects whether the highest scoring

label is correct, and Top-5 checks if the correct label appears in the top five predictions, as follows,

$$\text{Top-1} = \frac{1}{N} \sum_i \mathbf{1}_{\text{Top1}}(\mathbf{x}_i, y_i),$$

$$\text{Top-5} = \frac{1}{N} \sum_i \mathbf{1}_{\text{Top5}}(\mathbf{x}_i, y_i).$$

“Original label” accuracy measures alignment on the clean or unperturbed inputs (\uparrow is better), and “Target label” accuracy quantifies the misalignment with the adversary-specified target i.e. the *adversarial illusion attack success rate* (\downarrow is better).

Implementation details: All evaluations use the public ImageBind checkpoint without fine-tuning. Reconstruction-based defenses are applied to both original and perturbed images, and the resulting outputs are encoded with ImageBind to measure how effectively the defense restores semantic alignment.

Generative-based reconstruction: We adopt three pretrained generative models with different levels of capacity to reconstruct inputs and suppress adversarial artifacts. The **autoencoder (AE)** performs deterministic projection that removes high-frequency perturbations through latent-space compression. The **variational autoencoder (VAE)** introduces stochastic sampling in the latent space, enabling diverse reconstructions around the natural image manifold. The **diffusion model (DM)** further enhances reconstruction fidelity through iterative denoising, effectively restoring semantic content from perturbed inputs. All models are publicly available and used without fine-tuning. These generative priors map adversarial examples back onto the natural image manifold before re-encoding with ImageBind.

IV. RESULTS

A. Generative Mitigation Performance

Table I reports the performance of our proposed reconstruction-based mitigation method employing various generative models against adversarial illusion effects on the ImageBind multi-modal embedding model. For the baseline **without mitigation/attack (None)**, the original image achieves 85% Top-1 and 99% Top-5 accuracy with a CS of 1, confirming that clean samples are correctly classified by the downstream model. On the target label, these original clean images achieve only 0% Top-1 and 1% Top-5 accuracy, with a CS of 0.09 ± 0.05 , indicating that the model does not naturally align them with the attacker-chosen target. The original reconstructed sample, obtained by passing the image through ImageBind and then through BindDiffusion as a downstream reconstruction module, shows reduced performance with 42% Top-1 and 66% Top-5 accuracy, indicating that the reconstruction process introduces loss of class-specific details even in the absence of an attack. The perturbed image, which differs from the original only by an imperceptible perturbation, still reaches 77% Top-1 and 95% Top-5 accuracy on the original label, but its CS with the clean embedding drops to 0.11 ± 0.05 , showing that the perturbation significantly distorts the latent representation while leaving the image visually unchanged. On the target label, the same perturbed images obtain 0% for

TABLE I
EVALUATION OF GENERATIVE MITIGATION METHODS AGAINST ADVERSARIAL ILLUSION ON IMAGEBIND MULTI-MODAL EMBEDDING MODEL. TOP-1/TOP-5 ACCURACY AND CS ARE REPORTED FOR ORIGINAL AND PERTURBED IMAGES AND THEIR CORRESPONDING RECONSTRUCTIONS ON ORIGINAL AND TARGET LABELS.

Method	O/P	Original label			Target label		
		Top-1	Top-5	CS	Top-1	Top-5	CS
None	Org. Img.	85%	99%	1	0%	1%	0.09 ± 0.05
	Org. Rec.	42%	66%	-	0%	1%	-
	Prt. Img.	77%	95%	0.11 ± 0.05	0%	0%	0.72 ± 0.08
	Prt. Rec.	0%	0%	-	62%	90%	-
AE	Org. Img.	65%	89%	0.67 ± 0.09	0%	0%	0.09 ± 0.05
	Org. Rec.	18%	39%	-	0%	1%	-
	Prt. Img.	62%	82%	0.62 ± 0.10	0%	1%	0.10 ± 0.05
	Prt. Rec.	18%	35%	-	0%	0%	-
DM	Org. Img.	81%	98%	0.91 ± 0.04	0%	1%	0.09 ± 0.05
	Org. Rec.	39%	64%	-	0%	1%	-
	Prt. Img.	77%	95%	0.81 ± 0.08	0%	0%	0.11 ± 0.05
	Prt. Rec.	25%	53%	-	0%	1%	-
VAE	Org. Img.	84%	98%	0.93 ± 0.02	0%	1%	0.08 ± 0.05
	Org. Rec.	43%	67%	-	0%	1%	-
	Prt. Img.	78%	96%	0.82 ± 0.07	0%	1%	0.12 ± 0.05
	Prt. Rec.	22%	47%	-	0%	2%	-
DM + Sampling (Ours)	Org. Img.	80%	98%	0.92 ± 0.04	0%	1%	0.09 ± 0.05
	Org. Rec.	45%	73%	-	0%	1%	-
	Prt. Img.	77%	96%	0.81 ± 0.08	0%	1%	0.11 ± 0.05
	Prt. Rec.	34%	61%	-	0%	3%	-
VAE + Sampling (Ours)	Org. Img.	84%	98%	0.93 ± 0.02	0%	1%	0.08 ± 0.05
	Org. Rec.	46%	73%	-	0%	2%	-
	Prt. Img.	78%	96%	0.82 ± 0.07	0%	1%	0.12 ± 0.05
	Prt. Rec.	43%	68%	-	0%	2%	-

both Top-1 and Top-5 accuracies, with a CS of 0.72 ± 0.08 , indicating that the attack successfully shifts the embedding toward the adversary’s target even though the classifier does not yet predict it. Finally, the perturbed reconstructed sample, generated from the perturbed image via ImageBind and BindDiffusion, loses alignment with the true class (0% Top-1, 0% Top-5) and instead aligns with the attacker’s target (Top-1 = 62%, Top-5 = 90%), demonstrating that the illusion attack effectively transfers through the generative process and manipulates cross-modal semantics.

We see that **AE, DM, and VAE** mitigations are unable to sub-goal of retaining original label accuracy compared to the baseline without mitigation/attack (None) even though they achieve the sub-goal of minimizing the target label accuracy on perturbed images and improving the cosine similarity with the correct text label embeddings by reconstructing perturbed images.

We now explain our consensus-based generative sampling mitigation results. Here, we draw 10 samples from the VAE and DM per input. This choice is supported by Figure 2, which shows that both Top-1 and Top-5 accuracy plateau beyond roughly ten samples. Using 10 samples therefore balances robustness and computational cost while capturing the full benefit of consensus-based generative sampling. We find that **DM + Sampling** achieves strong robustness on adversarial illusion attacks and stable cross-modal alignment on original and perturbed inputs. Finally, we find that our **VAE + Sampling** configuration achieves the best overall reconstruction performance. The original image reaches 84% Top-1 and 98% Top-5 accuracy with a CS of 0.93 ± 0.02 .

TABLE II

COMPARISON OF OUR BEST-PERFORMING CONFIGURATION, I.E., VAE + SAMPLING, TO THE MITIGATION STRATEGIES INTRODUCED IN [35] UNDER THE ADVERSARIAL ILLUSION ATTACK ON THE IMAGEBIND MULTI-MODAL EMBEDDING MODEL. WE REPORT TOP-1/TOP-5 ACCURACY AND CS FOR ORIGINAL AND PERTURBED IMAGES AND THEIR RECONSTRUCTIONS ON ORIGINAL AND TARGET LABELS.

Method	O/P	Original label			Target label		
		Top-1	Top-5	CS	Top-1	Top-5	CS
None	Org. Img.	85%	99%	1	0%	1%	0.09 ± 0.05
	Org. Rec.	42%	66%	-	0%	1%	-
	Prt. Img.	77%	95%	0.11 ± 0.05	0%	0%	0.72 ± 0.08
	Prt. Rec.	0%	0%	-	62%	90%	-
JPEG	Org. Img.	84%	98%	0.91 ± 0.04	0%	1%	0.09 ± 0.05
	Org. Rec.	37%	55%	-	0%	1%	-
	Prt. Img.	79%	93%	0.78 ± 0.07	0%	1%	0.12 ± 0.05
	Prt. Rec.	25%	50%	-	0%	2%	-
Gaussian Blurred	Org. Img.	70%	89%	0.77 ± 0.05	0%	1%	0.09 ± 0.04
	Org. Rec.	29%	50%	-	0%	2%	-
	Prt. Img.	65%	87%	0.74 ± 0.07	0%	0%	0.10 ± 0.04
	Prt. Rec.	26%	53%	-	0%	0%	-
Random Affine	Org. Img.	83%	96%	0.84 ± 0.05	0%	0%	0.10 ± 0.05
	Org. Rec.	36%	61%	-	0%	0%	-
	Prt. Img.	81%	96%	0.78 ± 0.07	0%	0%	0.12 ± 0.04
	Prt. Rec.	32%	56%	-	0%	1%	-
Color Jitter	Org. Img.	83%	99%	0.88 ± 0.04	0%	1%	0.09 ± 0.05
	Org. Rec.	35%	60%	-	0%	1%	-
	Prt. Img.	76%	95%	0.60 ± 0.12	0%	0%	0.22 ± 0.06
	Prt. Rec.	12%	31%	-	1%	7%	-
Horizontal Flip	Org. Img.	84%	99%	0.90 ± 0.03	0%	1%	0.09 ± 0.05
	Org. Rec.	45%	66%	-	0%	1%	-
	Prt. Img.	77%	96%	0.66 ± 0.15	0%	1%	0.20 ± 0.08
	Prt. Rec.	17%	39%	-	0%	2%	-
Random Perspective	Org. Img.	72%	94%	0.80 ± 0.06	0%	0%	0.10 ± 0.05
	Org. Rec.	26%	54%	-	0%	1%	-
	Prt. Img.	74%	89%	0.73 ± 0.09	0%	0%	0.12 ± 0.04
	Prt. Rec.	25%	52%	-	0%	2%	-
VAE + Sampling (Ours)	Org. Img.	84%	98%	0.93 ± 0.02	0%	1%	0.08 ± 0.05
	Org. Rec.	46%	73%	-	0%	2%	-
	Prt. Img.	78%	96%	0.82 ± 0.07	0%	1%	0.12 ± 0.05
	Prt. Rec.	43%	68%	-	0%	2%	-

The reconstructed image maintains 46% Top-1 and 73% Top-5 accuracy, exceeding the baseline (None) for the same case, where no mitigation or attack is applied. This indicates that the proposed method does not introduce adverse effects under normal, non-adversarial conditions and can potentially improve performance. Under attack, the perturbed image achieves 78% Top-1 and 96% Top-5 accuracy with a CS of 0.82 ± 0.07 , while the reconstructed perturbed sample restores 43% Top-1 and 68% Top-5 accuracy. For comparison, in the normal system without mitigation (None), the reconstructed image from the original image achieves 42% Top-1 and 66% Top-5 accuracy. This indicates that VAE + Sampling mitigation can even surpass the accuracy and performance of the normal system under non-adversarial conditions. For the target label, cosine similarity remains very low at 0.08 ± 0.05 for the original image and 0.12 ± 0.05 for the perturbed image, and target-label accuracy stays near zero across all settings. These results show that adding stochastic sampling to the VAE further improves robustness by suppressing adversarial bias and encouraging smoother, reliable reconstructions.

B. Comparison with Other Mitigation Methods

Table II compares our generative reconstruction mitigation method with several standard image-level mitigation techniques, including JPEG compression, Gaussian blur, random

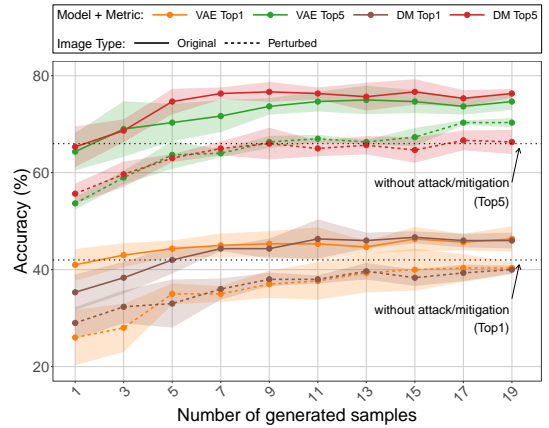


Fig. 2. Effect of sampling size on reconstruction robustness for VAE and DM mitigation methods. Dotted lines show baseline without attack/mitigation for Top-1/Top-5 accuracy. Increasing the number of generated samples during the generative sampling stage improves both Top-1 and Top-5 accuracy for original and perturbed images, with performance stabilizing beyond 10 generated samples.

affine transformation, color jitter, horizontal flip, and random perspective. These preprocessing-based methods operate directly in pixel space and are evaluated under the same adversarial illusion setup as our generative method.

State-of-the-art data augmentation methods provide only limited protection against adversarial illusions. JPEG compression and Gaussian blurring offer slight improvements, recovering 25% and 26% Top-1 accuracy on perturbed reconstructions, but they also reduce clean reconstruction accuracy to 37% and 29% respectively. Other augmentations such as random affine, color jitter, horizontal flip and random perspective show similar behavior. They partly disrupt the adversarial perturbation while introducing substantial semantic degradation. For example, random affine reconstruction recovers 32% Top-1 accuracy on perturbed inputs, and color jitter and random perspective yield only 12% and 25%. Cosine similarity to the original label drops sharply under these transformations, for instance 0.60 ± 0.12 for color jitter and 0.66 ± 0.15 for horizontal flip. In addition, color jitter produces elevated cosine similarity to the target label up to 0.22 ± 0.06 , indicating residual adversarial influence. In contrast, our **VAE + Sampling** defense achieves substantially higher recovery, restoring 43% Top-1 and 68% Top-5 accuracy on perturbed reconstructions while preserving strong clean-image performance and maintaining near-zero target-label alignment 0.12 ± 0.05 . Unlike deterministic pixel-level transformations, the generative model explicitly projects inputs back onto the natural data manifold, suppressing adversarial noise without removing class-relevant structure. These results show that generative mitigation provides a more principled and semantically grounded defense strategy that yields significantly stronger robustness.

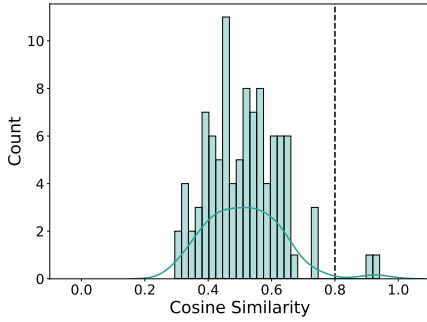


Fig. 3. Distribution of cosine similarities between perturbed embeddings and target labels across attack iterations. These results guide the selection of a cosine similarity threshold of 0.8.

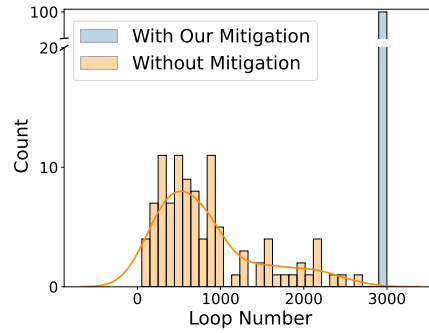


Fig. 4. Distribution of loop numbers for attacks with and without our mitigation. Incorporating our mitigation increases attack costs. With our mitigation, the attack is unsuccessful for all images after 3000 rounds.

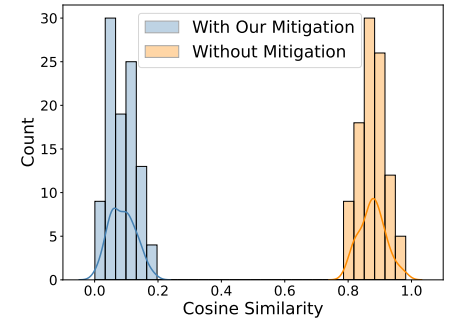


Fig. 5. Distribution of cosine similarities between perturbed embeddings and target labels. Attacks with our mitigation yield low cosine values, whereas attacks without it reach the maximum similarity threshold.

C. Mitigation Computational Overheads

Let us now discuss the trade-off between defense success rate and the computational overheads of our proposed defense mechanism. Figure 2 analyzes the effect of varying the number of generated samples used during the generative sampling stage for both VAE and DM models. As the number of generated samples increases, both Top-1 and Top-5 accuracies improve consistently for original and perturbed images. This indicates that aggregating over more samples provides a smoother and more reliable reconstruction of the input manifold, enhancing robustness against adversarial illusions. However, the trend stabilizes after approximately 10 samples, implying that beyond this point, additional sampling offers limited benefit relative to computational cost. The computational overheads of the VAE and DM are 0.3 ± 0.02 and 0.11 ± 0.18 seconds, respectively, which are both considered negligible compared to the processing pipeline in multi-modal models (multi-modal encoder, downstream task, and classifier) with 18.28 ± 0.79 seconds. This demonstrates that the overheads introduced by the VAE and DM are less than 2% of the entire processing pipeline we consider here. The number of parameters also follow a similar pattern. In particular, the VAE has 83.61 million parameters, which is marginal compared to the processing pipeline in multi-modal models with 2157.52 million parameters.

D. Attack Cost

In this section, we examine whether an attacker who has access to the generative model used in our mitigation can incorporate it into the attack generation loop to achieve a successful attack, and we evaluate the associated attack cost. The *attack cost* quantifies the difficulty of generating an adversarial illusion, measured by the number of optimization steps or model queries required for a successful attack. A higher attack cost indicates that the adversary must spend more computational or query resources to align the perturbed embedding with the target label, implying stronger robustness of the model or defense mechanism.

To measure attack cost, we quantify the number of optimization steps required to achieve a successful attack. First, we establish a criterion for determining when an attack should be considered successful. To do so, we conduct an experiment using the normal system without mitigation and run the attack optimization loop until the reconstructed image’s Top-1 prediction from the classifier matches the target class. At that point, we record the cosine similarity between the perturbed embedding and the target label.

The distribution of cosine similarities is shown in Fig. 3. This analysis allows us to identify a meaningful cutoff for when an attack can be considered successful, ensuring that comparisons of attack cost reflect genuine robustness rather than arbitrary stopping rules. The cosine similarities exhibit a mean of 0.52 ± 0.12 . Based on this distribution, we adopt a conservative threshold of 0.8, which covers approximately 98% of successful attacks. We also consider a maximum loop budget of 3000 iterations, as attacks that reach the threshold of 0.8 consistently achieve top-1 accuracy for the target label. If an attack does not reach the cosine similarity threshold within this loop count budget we record it as failed and assign the maximum loop count when reporting attack cost and plotting loop number histograms.

Using these thresholds, we evaluate attack cost under two settings in which attacks optimize through the VAE or operate directly in pixel space to compare the robustness gained from introducing the generative model. Incorporating the VAE into the attack loop increases the attack cost significantly. When the adversary optimizes through the VAE, perturbations must pass through the generative bottleneck before being evaluated by the encoder, which disrupts the gradient flow and constrains updates to the image manifold. Consequently, the attack converges slowly or fails entirely, leading to a high attack cost and low cosine similarity between the perturbed image and target label, e.g., most attacks reach the maximum of 3000 iterations with cosine similarity below 0.19, as shown in Figures 4 and 5. When the attack is applied directly in pixel space without the VAE, gradients propagate unimpeded, resulting in faster convergence, low attack cost, and high cosine similarity

with the target label, generally converging in fewer than 1000 iterations with cosine similarity above 0.8, which represents the maximum threshold. In our experiments, the model that includes the VAE consistently reaches the maximum loop budget without achieving the cosine similarity threshold, confirming that the generative constraint substantially limits the attack’s effectiveness. Figure 5 shows that when we continue the attack optimization loops for 3000 iterations, the cosine similarity between the perturbed image and the target label diverges sharply between the two settings. Without mitigation, the similarity approaches the target, whereas with our mitigation it remains far from it. This demonstrates that even when the attacker includes the VAE in the optimization loop, the attack fails to align the perturbed embedding with the target, indicating that our mitigation effectively prevents successful adversarial illusions.

E. Extension to Text Downstream Task

Figure 6 presents the results of extending the adversarial illusion analysis to a text-generation downstream task. For each input image, either original or perturbed, we generate a single textual description using the corresponding generative model (VAE or DM). We then compute the similarity between the generated text embedding and both the original and target label embeddings using the `all-mpnet-base-v2` model from the Sentence-Transformers library [21], based on MPNet [24].

The figure shows that across different number of generated samples, both VAE and DM maintain high similarity with the original label for clean images (solid lines), while adversarial perturbations (dashed lines) reduce this alignment slightly but consistently. Meanwhile, the similarity with the target label (green and red lines) remains low, indicating that the generative defenses largely prevent semantic transfer to the attacker-specified target. DM-based reconstructions (brown and red) achieve slightly higher stability than the VAE across all sampling sizes, demonstrating more consistent text alignment under adversarial conditions. Varying the number of generated samples shows no significant improvement, suggesting that a single generated sample per image is sufficient to capture the dominant semantic alignment for text-level evaluation.

V. RELATED WORK

Multi-modal models integrate information from multiple modalities, such as images and text, to learn unified representations for cross-modal tasks [19, 25, 34]. Unlike traditional adversarial perturbations that shift decision boundaries, adversarial illusions exploit cross-modal embedding misalignment, causing unrelated modalities to appear aligned in joint representation spaces [35]. For instance, Zhang et al. [35] demonstrated that imperceptibly perturbed images could align with semantically unrelated text in models such as ImageBind and AudioCLIP, misleading both image and text generation pipelines without knowledge of the specific downstream tasks. Recent embedding-space and diffusion-guided attacks further highlight this vulnerability in vision-language models [12, 23].

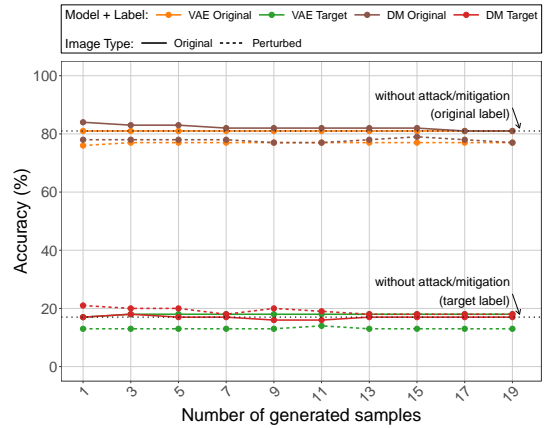


Fig. 6. Effect of sampling size on text generation downstream task accuracy for VAE and DM mitigation methods. Dotted lines show baseline without attack/mitigation for the original and target labels. Accuracy for both original and target labels is reported across varying number of generated samples. Increasing the number of generated samples has a minor impact on text alignment accuracy.

Because adversarial illusions manipulate cross-modal alignment rather than decision boundaries, unimodal defenses that preserve label accuracy may still fail to maintain alignment across modalities, motivating generative approaches to restore shared embeddings. Thus, maintaining robust cross-modal alignment has emerged as a distinct challenge beyond unimodal adversarial robustness [6, 29, 36].

Beyond attacks that directly manipulate image–text embeddings, recent work has shown that adversarial images can reliably steer large multi-modal systems. Wu et al. [28] found that a single optimized trigger image can mislead web agents by forcing captioners or CLIP encoders to output attacker-chosen descriptions, which then propagate through downstream decision pipelines. A complementary line of work constructs universal adversarial images that jailbreak multi-modal LLMs across many prompts by optimizing through the vision–language stack [20]. These attacks assume gradient access to at least part of the multi-modal pipeline and target agent or language model behavior directly. Our setting differs because we evaluate reconstruction-based defenses under a black-box setting, where the attacker cannot optimize through or modify the generative reconstructor.

Early heuristic defenses such as feature squeezing and JPEG-based transformations [5, 10, 32] inspired the use of autoencoders as learned reconstruction-based purifiers. Convolutional AEs have been widely studied as defenses against adversarial perturbations, aiming to remove input-space perturbations before classification [1]. Early frameworks such as Magnet attempted to detect and reconstruct adversarial samples but remained vulnerable to adaptive white-box attacks [17]. Denoising AEs introduced robust latent representations [27] and later outperformed traditional filtering for tasks like facial denoising [4]. Although effective for image restoration, these approaches have not been systematically evaluated under adversarial illusions, where the goal is preserving cross-modal

alignment rather than unimodal fidelity.

VAEs extend AEs with probabilistic latent spaces, enabling structured representations that can regularize noisy inputs [13]. The Adversarial Symmetric VAE introduced adversarial training to improve reconstruction and robustness [18], while more recent gated recurrent VAEs have been used in industrial control systems for generating and defending against adversarial samples [30]. Defensive variants such as AdMVAE [33] and Def-VAE [15] further demonstrate that probabilistic latent models can suppress adversarial signals in unimodal domains. However, the potential of these models for cross-modal alignment recovery, which is a key requirement in adversarial illusion scenarios, remains largely unexplored.

Generative DMs have recently emerged as powerful tools for defending against adversarial attacks, particularly in multi-modal settings. By iteratively denoising inputs in a learned latent space, DMs can restore both perceptual quality and semantic alignment [29]. Frameworks such as DiffDf [31], ADBM [14], gradient-free purification [3], and DiffCAP [7] illustrate the growing use of diffusion-based purification for robustness. Compared to AE- or VAE-based methods, diffusion approaches provide greater flexibility and alignment recovery but incur higher computational cost. These advances suggest that generative purification may offer a promising path toward defending cross-modal representations from adversarial illusions.

Our consensus-based generative mitigation in this paper, by integrating reconstruction, stochastic sampling, and majority aggregation, reduces the adversarial illusions success rate to near-zero, while improving cross-modal alignment in unperturbed input settings without any attack/mitigation as well as in perturbed input settings compared to the existing solutions.

VI. CONCLUSIONS

We provide a consensus-based generative mitigation against adversarial illusions in multi-modal models and demonstrate their efficacy on image and text downstream tasks. Since our defense requires no additional training, it can be deployed readily in the state-of-the-art multi-modal models. Our experiments on the state-of-the-art multi-modal encoders show that our approach substantially reduces the attack success rates and improves cross-modal alignment, providing an effective and model-agnostic defense against adversarial illusions.

ACKNOWLEDGMENT

This work is partially supported by the Wallenberg AI, Autonomous Systems and Software Program (WASP) funded by the Knut and Alice Wallenberg Foundation, the Swedish Research Council, and by an unrestricted gift from Google.

REFERENCES

- [1] Syeda Nazia Ashraf, Raheel Siddiqi, and Humera Farooq. Auto encoder-based defense mechanism against popular adversarial attacks in deep learning. *PloS one*, 19(10): e0307363, 2024.
- [2] Anish Athalye, Nicholas Carlini, and David Wagner. Obfuscated gradients give a false sense of security: Circumventing defenses to adversarial examples. In *International conference on machine learning*, pages 274–283. PMLR, 2018.
- [3] Xuelong Dai, Dong Wang, Duan Mingxing, and Bin Xiao. Gradient-free adversarial purification with diffusion models. *arXiv preprint arXiv:2501.13336*, 2025.
- [4] Muazzez Buket Darıcı and Zeki Erdem. A comparative study on denoising from facial images using convolutional autoencoder. *Gazi University Journal of Science*, 36(3):1122–1138, 2023.
- [5] Nilaksh Das, Madhuri Shanbhogue, Shang-Tse Chen, Fred Hohman, Siwei Li, Li Chen, Michael E Kounavis, and Duen Horng Chau. Shield: Fast, practical defense and vaccination for deep learning using jpeg compression. In *Proceedings of the 24th ACM SIGKDD International Conference on Knowledge Discovery & Data Mining*, pages 196–204, 2018.
- [6] Zhihao Dou, Xin Hu, Haibo Yang, Zhuqing Liu, and Minghong Fang. Adversarial attacks to multi-modal models. In *Proceedings of the 1st ACM Workshop on Large AI Systems and Models with Privacy and Safety Analysis*, LAMPS '24, page 35–46, New York, NY, USA, 2024. Association for Computing Machinery. ISBN 9798400712098. doi: 10.1145/3689217.3690619. URL <https://doi.org/10.1145/3689217.3690619>.
- [7] Jia Fu, Yongtao Wu, Yihang Chen, Kunyu Peng, Xiao Zhang, Volkan Cevher, Sepideh Pashami, and Anders Holst. Diffcap: Diffusion-based cumulative adversarial purification for vision language models. *arXiv preprint arXiv:2506.03933*, 2025.
- [8] Rohit Girdhar, Alaaeldin El-Nouby, Zhuang Liu, Mannat Singh, Kalyan Vasudev Alwala, Armand Joulin, and Ishan Misra. Imagebind: One embedding space to bind them all. In *Proceedings of the IEEE/CVF conference on computer vision and pattern recognition*, pages 15180–15190, 2023.
- [9] Ian J Goodfellow, Jonathon Shlens, and Christian Szegedy. Explaining and harnessing adversarial examples. *arXiv preprint arXiv:1412.6572*, 2014.
- [10] Chuan Guo, Mayank Rana, Moustapha Cisse, and Laurens Van Der Maaten. Countering adversarial images using input transformations. *arXiv preprint arXiv:1711.00117*, 2017.
- [11] Chao Jia, Yinfei Yang, Ye Xia, Yi-Ting Chen, Zarana Parekh, Hieu Pham, Quoc Le, Yun-Hsuan Sung, Zhen Li, and Tom Duerig. Scaling up visual and vision-language representation learning with noisy text supervision. In *International conference on machine learning*, pages 4904–4916. PMLR, 2021.
- [12] Hanguo Kang, Jehyeok Yeon, and Gagandeep Singh. Trap: Targeted redirecting of agentic preferences. *arXiv preprint arXiv:2505.23518*, 2025.
- [13] Diederik P Kingma and Max Welling. Auto-encoding variational bayes. *arXiv preprint arXiv:1312.6114*, 2013.

- [14] Xiao Li, Wenxuan Sun, Huanran Chen, Qiongxiu Li, Yining Liu, Yingzhe He, Jie Shi, and Xiaolin Hu. Adbm: Adversarial diffusion bridge model for reliable adversarial purification. *arXiv preprint arXiv:2408.00315*, 2024.
- [15] Tengfei Lu, Zhongli Wang, Yan Shen, Xiaotao Shao, and Yonglin Tang. Defvae: A defect detection method for catenary devices based on variational autoencoder. *IEEE Transactions on Instrumentation and Measurement*, 72: 1–12, 2023.
- [16] Aleksander Madry, Aleksandar Makelov, Ludwig Schmidt, Dimitris Tsipras, and Adrian Vladu. Towards deep learning models resistant to adversarial attacks. *arXiv preprint arXiv:1706.06083*, 2017.
- [17] Dongyu Meng and Hao Chen. Magnet: a two-pronged defense against adversarial examples. In *Proceedings of the 2017 ACM SIGSAC conference on computer and communications security*, pages 135–147, 2017.
- [18] Yuchen Pu, Weiyao Wang, Ricardo Henao, Liqun Chen, Zhe Gan, Chunyuan Li, and Lawrence Carin. Adversarial symmetric variational autoencoder. *Advances in neural information processing systems*, 30, 2017.
- [19] Alec Radford, Jong Wook Kim, Chris Hallacy, Aditya Ramesh, Gabriel Goh, Sandhini Agarwal, Girish Sastry, Amanda Askell, Pamela Mishkin, Jack Clark, et al. Learning transferable visual models from natural language supervision. In *International conference on machine learning*, pages 8748–8763. PmLR, 2021.
- [20] Temurbek Rahmatullaev, Polina Druzhinina, Nikita Kurdiukov, Matvey Mikhailchuk, Andrey Kuznetsov, and Anton Razzhigaev. Universal adversarial attack on aligned multimodal llms. *arXiv preprint arXiv:2502.07987*, 2025.
- [21] Nils Reimers and Iryna Gurevych. Sentence-bert: Sentence embeddings using siamese bert-networks. *arXiv preprint arXiv:1908.10084*, 2019.
- [22] Christian Schlarmann, Naman Deep Singh, Francesco Croce, and Matthias Hein. Robust clip: Unsupervised adversarial fine-tuning of vision embeddings for robust large vision-language models. *arXiv preprint arXiv:2402.12336*, 2024.
- [23] Erfan Shayegani, Yue Dong, and Nael Abu-Ghazaleh. Jailbreak in pieces: Compositional adversarial attacks on multi-modal language models. *arXiv preprint arXiv:2307.14539*, 2023.
- [24] Kaitao Song, Xu Tan, Tao Qin, Jianfeng Lu, and Tie-Yan Liu. MpNet: Masked and permuted pre-training for language understanding. *Advances in neural information processing systems*, 33:16857–16867, 2020.
- [25] Nitish Srivastava and Russ R Salakhutdinov. Multimodal learning with deep boltzmann machines. *Advances in neural information processing systems*, 25, 2012.
- [26] Florian Tramèr, Alexey Kurakin, Nicolas Papernot, Ian Goodfellow, Dan Boneh, and Patrick McDaniel. Ensemble adversarial training: Attacks and defenses. *arXiv preprint arXiv:1705.07204*, 2017.
- [27] Pascal Vincent, Hugo Larochelle, Yoshua Bengio, and Pierre-Antoine Manzagol. Extracting and composing robust features with denoising autoencoders. In *Proceedings of the 25th international conference on Machine learning*, pages 1096–1103, 2008.
- [28] Chen Henry Wu, Jing Yu Koh, Ruslan Salakhutdinov, Daniel Fried, and Aditi Raghunathan. Adversarial attacks on multimodal agents. *arXiv e-prints*, pages arXiv–2406, 2024.
- [29] Chengwei Xia, Fan Ma, Ruijie Quan, Kun Zhan, and Yi Yang. Adversarial-guided diffusion for multimodal llm attacks. *arXiv preprint arXiv:2507.23202*, 2025.
- [30] Lijuan Xu, Zhi Yang, Dawei Zhao, Fuqiang Yu, Yang Zhou, and Hu Zhang. G-vae: Variational autoencoder-based adversarial attacks and defenses in industrial control systems. *Computers and Electrical Engineering*, 124: 110290, 2025.
- [31] Long Xu, Peng Gao, Wen-Jia Tang, Fei Wang, and Ru-Yue Yuan. Towards effective and efficient adversarial defense with diffusion models for robust visual tracking. *Information Fusion*, 124:103384, December 2025. ISSN 1566-2535. doi: 10.1016/j.inffus.2025.103384. URL <http://dx.doi.org/10.1016/j.inffus.2025.103384>.
- [32] Weilin Xu, David Evans, and Yanjun Qi. Feature squeezing: Detecting adversarial examples in deep neural networks. *arXiv preprint arXiv:1704.01155*, 2017.
- [33] Sheng-lin Yin, Xing-lan Zhang, and Li-yu Zuo. Defending against adversarial attacks using spherical sampling-based variational auto-encoder. *Neurocomputing*, 478: 1–10, 2022.
- [34] Xin Yuan, Zhe Lin, Jason Kuen, Jianming Zhang, Yilin Wang, Michael Maire, Ajinkya Kale, and Baldo Faieta. Multimodal contrastive training for visual representation learning. In *Proceedings of the IEEE/CVF conference on computer vision and pattern recognition*, pages 6995–7004, 2021.
- [35] Tingwei Zhang, Rishi Jha, Eugene Bagdasaryan, and Vitaly Shmatikov. Adversarial illusions in multi-modal embeddings. In *33rd USENIX Security Symposium (USENIX Security 24)*, pages 3009–3025, 2024.
- [36] Ziqi Zhou, Shengshan Hu, Minghui Li, Hangtao Zhang, Yechao Zhang, and Hai Jin. Advclip: Downstream-agnostic adversarial examples in multimodal contrastive learning. In *Proceedings of the 31st ACM International Conference on Multimedia*, pages 6311–6320, 2023.